ADVANCED MATERIALS
www.advmat.de

Digital Light Process 3D Printing of Magnetically Aligned Liquid Crystalline Elastomer Free–forms

Jeremy A. Herman, Rodrigo Telles, Caitlyn C. Cook, Samuel C. Leguizamon, Jennifer A. Lewis, Bryan Kaehr, Timothy J. White, and Devin J. Roach**

Liquid crystalline elastomers (LCEs) are anisotropic soft materials capable of large dimensional changes when subjected to a stimulus. The magnitude and directionality of the stimuli-induced thermomechanical response is associated with the alignment of the LCE. Recent reports detail the preparation of LCEs by additive manufacturing (AM) techniques, predominately using direct ink write printing. Another AM technique, digital light process (DLP) 3D printing, has generated significant interest as it affords LCE free-forms with high fidelity and resolution. However, one challenge of printing LCEs using vat polymerization methods such as DLP is enforcing alignment. Here, we document the preparation of aligned, main-chain LCEs via DLP 3D printing using a 100 mT magnetic field. Systematic examination isolates the contribution of magnetic field strength, alignment time, and build layer thickness on the degree of orientation in 3D printed LCEs. Informed by this fundamental understanding, DLP is used to print complex LCE free-forms with through-thickness variation in both spatial orientations. The hierarchical variation in spatial orientation within LCE free-forms is used to produce objects that exhibit mechanical instabilities upon heating. DLP printing of aligned LCEs opens new opportunities to fabricate stimuli-responsive materials in form factors optimized for functional use in soft robotics and energy absorption.

1. Introduction

Liquid crystalline elastomers (LCEs) are lightly cross-linked polymer networks that retain liquid crystallinity. The assimilation of anisotropy and viscoelasticity underpins the potential functional utility of LCEs in soft robotics,[1,2] impact resistance,[3–8] optics,[9–12] and energy.[13–16] Numerous prior reports detail the synthesis, alignment, deformation mechanics, and physics of LCEs.[17–20] The recent resurgence in LCE research is largely attributable to the introduction of facile materials chemistries that not only allow for straight-forward preparation of LCEs, but are also amenable to surface-enforced alignment,[21] mechanical alignment,[22] and rheological alignment.[23–26] Rheological alignment typically refers to the preparation of LCEs via direct ink write (DIW) 3D printing. In this method, a viscous LC oligomer melt is extruded through a nozzle onto a print bed where it is typically photopolymerized. The shear forces involved with extruding the ink through the nozzle impart alignment on the extruded filament, and subsequent photopolymerization locks in that alignment. Since the introduction of this method, there has been a surge in publications on DIW printing of LCEs. While DIW printing of LCEs has produced more complex alignment and shape changes than anything seen in these materials previously, most examples still are limited to flat films that actuate into 3D structures (2D to 3D shape transformation). Recent publications have detailed methods of printing 3D structures using DIW; however, these methods utilize pre-built-in support structures[27] or embedded printing in a gel media.[28] Nevertheless, DIW is a more accomplished technique and remains the fastest and most versatile method of preparing thick LCE actuators with complex director profiles. The complexity of larger 3D structures achievable by DIW is its biggest downside and this is where vat polymerization technologies such as digital light processing (DLP) are advantageous. There is an excellent review article that describes the differences in extrusion and vat polymerization techniques for the 3D printing of LCEs.[29]

DLP is an increasingly widespread vat polymerization method for producing complex 3D structures using additive manufacturing.[4,30] In this method, a liquid crystal (LC)(7):69 oligomer resin is poured into a vat and then photopolymerized

J. A. Herman, S. C. Leguizamon, B. Kaehr, D. J. Roach
Advanced Materials Laboratory
Sandia National Laboratories
Albuquerque, NM 87106, USA
E-mail: devin.roach@oregonstate.edu
J. A. Herman, T. J. White
Department of Chemical and Biological Engineering
University of Colorado
Boulder, CO 80303, USA
E-mail: tim.white@colorado.edu
R. Telles, J. A. Lewis
John A. Paulson School of Engineering and Applied Sciences and Wyss Institute for Biologically Inspired Engineering
Harvard University
Cambridge, MA 02138, USA
C. C. Cook
Lawrence Livermore National Laboratory
Livermore, CA 94550, USA
D. J. Roach
School of Mechanical, Industrial, and Manufacturing Engineering
Oregon State University
Corvallis, OR 97331, USA

The ORCID identification number(s) for the author(s) of this article can be found under https://doi.org/10.1002/adma.202414209

DOI: 10.1002/adma.202414209

layer by layer until a 3D structure is made. This method has been used to print 3D LCE lattice structures with exceptional resolution.[4,5] These LCE lattices have shown strong potential as energy-absorbing materials because of their combination of viscoelasticity and mesogen reorientation, also known as soft elasticity. Both polymer chain viscoelasticity and soft elasticity of LC mesogens provide mechanisms of dissipating energy. In traditional elastomers, only polymer chain viscoelasticity contributes to their energy dissipation mechanism. In previous examples of DLP printing LCEs, toluene is included in the resin to reduce its viscosity for room-temperature printing. This is a necessary step but is not ideal as toluene disrupts LC interactions. The most notable drawback of DLP printing for LCEs, however, is that the printed structures are typically unaligned, eliminating many of the primary advantages offered by LCEs.[31] Some researchers have attempted to solve this challenge by using a specialty-made printer that shears an entire layer of LC resin and then subsequently photopolymerizes it.[30] In this example, only bending actuation was seen in the shear-aligned and DLP-printed LCE films instead of the classic linear actuation response. Nevertheless, an alignment method that can be integrated into DLP printing and that is easily adjustable to form more complex shapes and actuation properties would open the door to a myriad of functional LCE structures.

Other procedures exist to achieve more complex alignment in LCEs, including photopatterned alignment[32–34] and electric field alignment.[35–38] Electric field alignment could potentially be integrated with DLP printing but is hindered by the need for high-strength electric fields (0.3 V μm^{-1}) which has only been used to print very small structures (100 µm).[35] One alignment method that has garnered much less attention, but is suitable for integration with DLP printing is magnetic field alignment.[39,40] Liquid crystals have an inherent diamagnetic susceptibility with the majority of mesogens aligning their long axis parallel to a magnetic field. The alignment of LCEs via a magnetic field has been minimal compared to other alignment methods and has mostly been used to align side-chain LCEs[41–43] with some examples shown to align a main-chain LCE using high-strength magnetic fields and long alignment times.[44,45] For this work, our studies focus on main-chain LCE formulations as they achieve greater length changes in their actuation and possess superior viscoelastic properties as compared with side-chain LCEs.[46]

Motivated by the potential to prepare free–form LCEs with spatial and hierarchical variation in director orientation and informed by a recent report,[47] we demonstrate the preparation of very thick aligned LCE free–forms, up to 70 layers and 7 mm tall. The LCEs are aligned by a low-strength magnetic field (100 mT) generated by a Halbach array that can be integrated with a commercially available DLP printer. The LCEs are prepared via a dual-stage thiol-acrylate/thiol-ene materials chemistry placed in a liquid crystalline solvent 4-Cyano-4′-pentylbiphenyl (5CB). The association of director orientation and variables relating to magnetic field alignment such as field strength, alignment time, and layer thickness are systematically explored. This fundamental understanding is the basis of subsequent studies to prepare 3D-printed free–forms to include LCEs with spatial and hierarchical variance in director orientation. In this way, this contribution is an advance in demonstrating that LCEs can be prepared by DLP printing to prepare complex 3D free–forms with potential for paradigm-shift in soft robotics, dynamic structures, and energy absorption.

2. Results and Discussion

LCEs were prepared via sequential thiol-Michael oligomerization and thiol-ene photopolymerization.[48–50] The LCE composition was based on the commercially available liquid crystalline (LC) monomer C6M (**Figure 1a**). The polymerizable LCE composition was mixed with the non-reactive LC molecule 4-Cyano-4′-pentylbiphenyl (5CB, Figure 1a) in a 1:1.5 weight ratio. Thiol-Michael oligomerization of C6M with the chain extending dithiol 2,2′-(Ethylenedioxy)diethanethiol (EDDT, Figure 1a) was catalyzed with dipropylamine (DPA, Figure 1a). The formulation contains a molar excess of thiols and accordingly, the thiol-Michael addition reaction produces thiol-terminated C6M oligomers. The oligomeric composition is viscous and retains liquid crystallinity, also known as the nematic phase. In a comparative study, non-liquid crystalline oligomeric compositions did not align with a magnetic field (Table S1, Supporting Information). 5CB is included in the mixture to reduce the viscosity of the resin, increase the robustness of the nematic phase, and improve the affinity of the mixture to magnetic field alignment. 5CB and C6M both possess positive values of diamagnetic susceptibility, meaning they will both orient their long axis parallel to the applied magnetic field.[51] Overall, the resin with 5CB included will have a stronger diamagnetic response than if a non-liquid crystalline, isotropic solvent (such as toluene) was included.

Aligned, main-chain LCEs were prepared from this composition by exposure to a magnetic field. The magnetic field was produced from magnets arranged in a Halbach array (Figure 1b) where cubic magnets were integrated into a 3D-printed housing. The magnetic poles were aligned to produce a uniform magnetic field that is unidirectional. The red arrows on each magnet point toward their north pole. Collectively, the magnets of the Halbach array produce a magnetic field of 100 mT that points in a single direction marked by the nematic director, n (Figure 1b). The consistency in the orientation of the magnetic field is visualized in the alignment of magnetic particles in Figure S1a (Supporting Information). The diamagnetic susceptibility of LC molecules and monomers results in alignment parallel to the magnetic field (Figure 1b). The inclusion and concentration of 5CB are critical in enabling alignment as compared to formulations using toluene as the solvent or formulations where the 5CB content is increased or decreased (Figure S2, Supporting Information). Upon magnetic field alignment, the oligomeric composition is photopolymerized by reacting excess thiol groups with unreacted tetrafunctional vinyl cross-linker glyoxal bis(diallyl acetal) (GDA, Figure 1a) which arrests the alignment. The result is an LCE that retains uniaxial alignment.

This alignment is evident as seen using wide-angle X-ray scattering (WAXS) and in the material's thermomechanical response (Figure 1c). Upon heating and under isostress conditions, the LCE film contracts parallel to the aligned axis (negative strain) and expands orthogonal to the aligned axis (Figure S3, Supporting Information). The aligned LCE film repeatedly exhibits 25–30% strain over many cycles (Figure S4, Supporting Information). Comparatively, an LCE film prepared without magnetic field alignment does not exhibit directional actuation (Figure 1c).

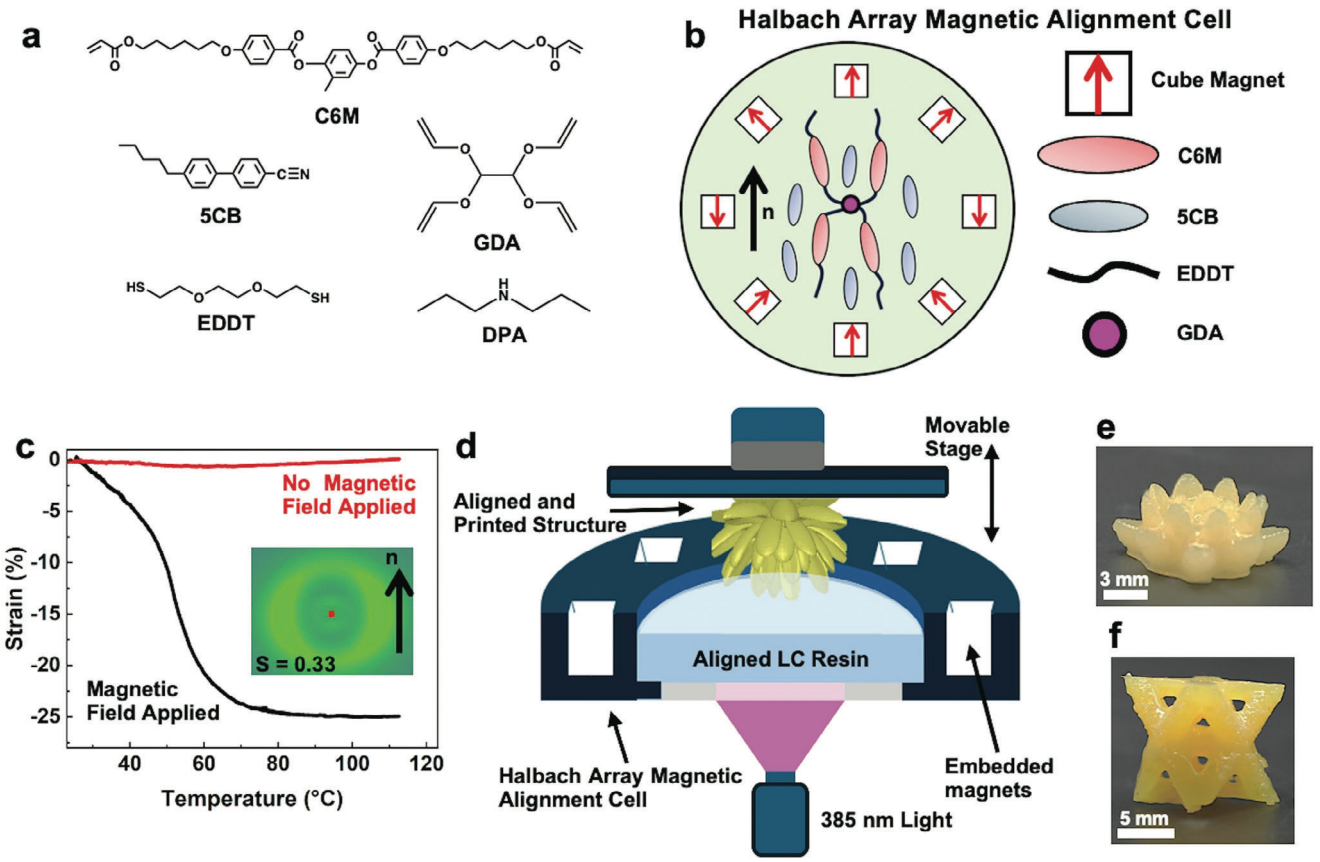

Figure 1. a) Chemical structures of liquid crystalline diacrylate (C6M), liquid crystalline solvent (5CB), dithiol (EDDT), tetraene (GDA), and amine (DPA) are illustrated. b) A viscous mixture of the oligomers and LC solvent is aligned by placing into a magnetic Halbach array. The arrangement of the cubed magnets produces a uniform 100 mT field. Upon alignment, the mixture is photopolymerized to form an aligned LCE. Red arrows points toward the north pole on each magnet of the Halbach array while the black arrow corresponds to the nematic director. c) The alignment of the LCE results in films that exhibit directional actuation associated with orientational order. WAXS scan (inset) is shown of aligned sample with calculated orientation parameter (S). d) The Halbach array can be integrated with a bottom-up DLP printer to 3D print aligned structures. e) A lotus flower composed of LCE is printed as an illustration. f) A single octet truss unit cell is printed. 3D printed LCEs have been identified as low-density energy-absorbing materials and alignment integrated with a lattice structure should enhance dissipation in these materials.

This alignment of the LCE is evident in the WAXS pattern shown in Figure 1c. The Herman's orientation parameter (S) for this LCE was calculated to be 0.33, which is comparable to prior reports of aligned LCEs where orientation parameters between 0.3–0.6 are typically reported.[52,53] The composition and magnetic field alignment were then integrated with a commercially available DLP printer (Figure S5, Supporting Information). The DLP printer exposes the material with 385 nm light projected from the bottom of the vat filled with the LC composition. The Halbach array is placed around the vat to align the resin before the build layer is printed (Figure 1d). This approach allows for the printing of complex 3D free–form objects that take advantage of the fidelity of DLP, such as a lotus flower (Figure 1e) and an octet truss lattice unit cell (Figure 1f). The combination of an anisotropic material like aligned LCEs with lattice geometries like an octet truss could lead to enhanced energy absorption properties in low-density, soft materials.

Prior reports have employed comparatively high-strength magnetic fields (500–1000 mT) to align LC precursors before polymerization. We fabricated additional alignment arrays to produce fields of 50 and 200 mT to better understand the association of magnetic field strength and alignment. In a previous report where side-chain LCEs are magnetically aligned, maximal alignment is achieved at a 100 mT field strength,[41] which corresponds well to the results for our system (**Figure 2a**). The film aligned with the 200 mT field reaches the same actuation amount. However, when the magnetic field strength is reduced to 50 mT, the material does not align to the same amount and reach the same actuation (Figure 2a). A Frederiks threshold is the field strength necessary to align a liquid crystalline director and this threshold is dependent on the system being studied.[51] For this system, a 100 mT field strength results in the full alignment we achieve when alignment time and film thickness are held constant.

A higher-strength magnetic field, however, can work to align thicker samples and, by extension, offers the opportunity to print thicker build layers and accelerate the printing of large architectures. To show this, the oligomeric resin was aligned in the 100 and 200 mT arrays for 5 min and the film thicknesses were varied (100, 250, 500, and 750 μm). For simplicity, the maximum

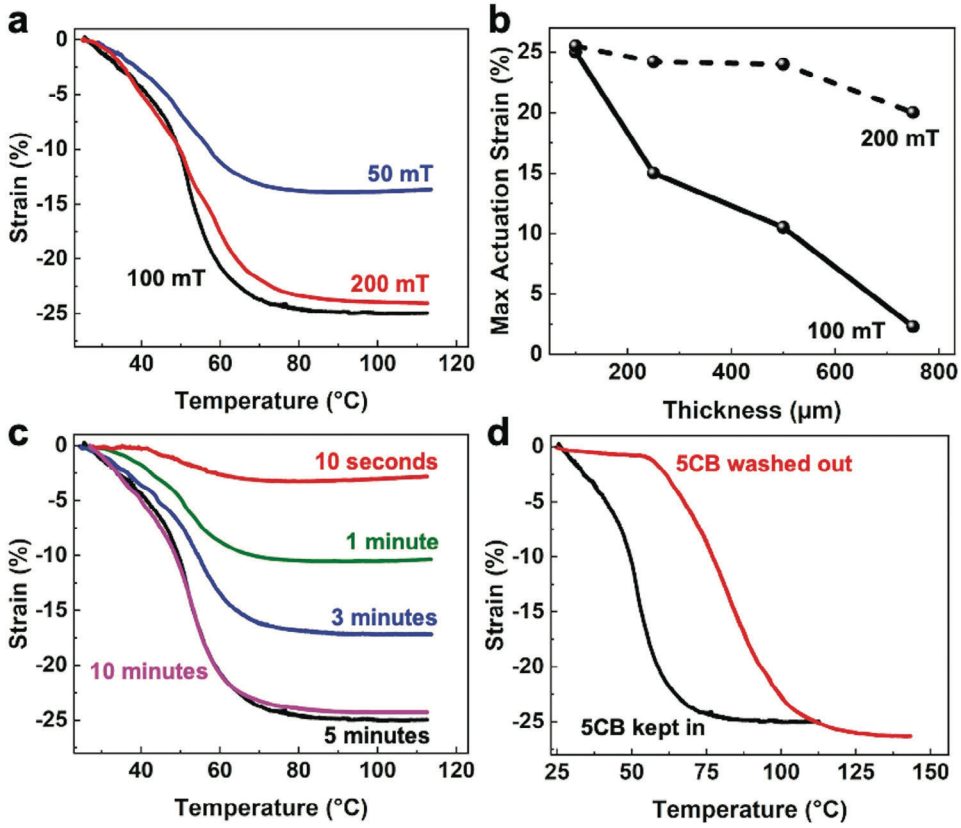

Figure 2. a) The thermomechanical response of LCEs depends on the field strength. All samples were aligned for 5 min and are 100 μm thick. b) Summary of experiments examining the thermomechanical response of LCEs prepared over a range of thicknesses subject to alignment at 100 and 200 mT. All samples were aligned for 5 min. c) Thermomechanical response of LCEs subject to 100 mT magnetic field alignment for time ranging from 10 s to 10 min. All samples are 100 μm thick. d) Thermomechanical response of the LCE with 5CB as plasticizer or after washing.

actuation strain of each material versus their thickness is plotted and shown in Figure 2b (full examination shown in Figure S6a,b, Supporting Information). Increasing the field strength allows for better alignment of thicker LCEs.

The time to reach alignment of our LCE system was also considered and studied using the 100 mT Halbach array. As shown in Figure 2c, 5 min of alignment time was necessary to reach the maximum alignment (maximum uniaxial actuation) for this system. A 10-min alignment time did not offer any additional actuation as seen in the overlapping 5-min and 10-min curves. Going below 5 min, however, saw a decrease in the alignment and reduced the actuation contraction of the materials. A similar alignment time study was done using the 200 mT array and shown in Figure S6c (Supporting Information). While the 200 mT array offered minor improvements to the alignment compared to the 100 mT array, we saw a similar overall trend and concluded that a 5-min alignment time using the 100 mT Halbach array was sufficient for the rest of our studies and integration with DLP printing.

The inclusion of the low molar mass LC 5CB is critical for enabling alignment but also affects the thermomechanical properties of the LCE, as evident in Figure 2d. Explicitly, the nonreactive 5CB acts as a plasticizer to the LCE after cross-linking. Comparatively, the thermomechanical response of the LCE plasticized with 5CB occurs at lower temperatures than when 5CB is removed by solvent exchange and drying (with DCM). The washed material exhibits a higher T_{NI} (Figure S7a, Supporting Information) and an increased modulus (Figure S7b, Supporting Information) than the unwashed material. Even with the removal of 5CB, the alignment is retained as evidenced by the thermomechanical actuation behavior shown in Figure 2d. Scanning electron microscopy (SEM) on the washed and unwashed films indicated that the removal of 5CB did not leave any porosity in the film (Figure S8, Supporting Information). We also measured the volume and mass change of these samples when 5CB was removed and noticed that the density of the material stayed the same (Table S2, Supporting Information).

Informed by experiments assessing the alignment of LCE films in a magnetic field, we subsequently explore the voxelation of LCE free–forms by DLP printing. For consistency, we use the 100 mT Halbach array for magnetic alignment, aligned each build layer for 5 min, and prepared build layers of 100 μm thickness. Given the differences in the processing environment, the DLP-printed LCEs exhibit a slight increase in modulus and a higher temperature thermomechanical response (Figure S9, Supporting Information). Subsequently, we prepared multi-layer DLP prints of LCEs. As shown in Figure 3a, a two-layer print is prepared of a uniaxially aligned layer printed on top of an unaligned layer. Upon heating, the bilayer LCE print curls due to the alignment mismatch between the material layers and through the material thickness. WAXS scans of the varying individual

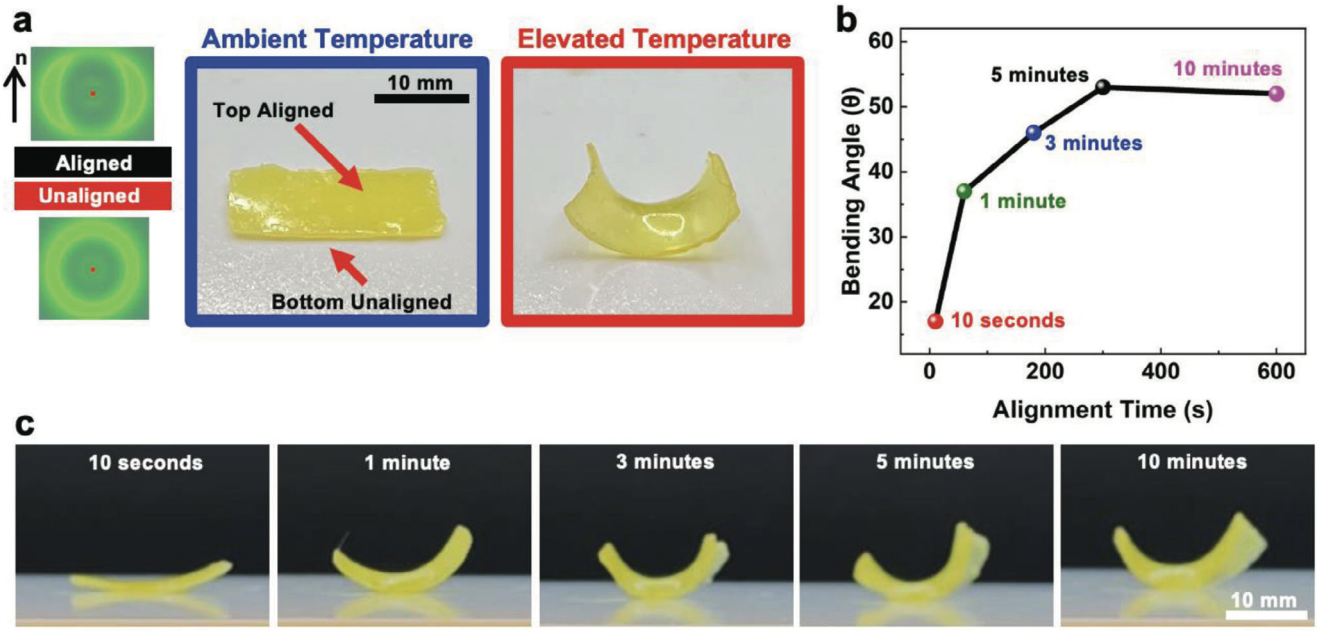

Figure 3. a) A bilayer LCE was 3D printed where half of the film is aligned and half of the film is unaligned. WAXS scans illustrate the anisotropy in the aligned side and isotropy in the unaligned side. The originally flat film curls when heated. b) The thermomechanical response of the LCE bilayer is summarized by measured bending angle as a function of alignment time. Again, increasing the time for magnetic field alignment enables greater orientation and enhanced response. c) The deformation of the bilayer elements are visualized in photographs as a function of magnetic field alignment time.

layers indicate anisotropy in the aligned layer and an isotropic halo scattering pattern in the unaligned layer (**Figure** 3a). To illustrate the influence of alignment time in preparing multi-layer DLP LCEs, we prepared elements in which the alignment was facilitated by 100 mT exposure for 10 s to 10 min. The influence of alignment time on director orientation is evident in the summary of the bending angle (Figure 3b) taken from the stimuli-response of the DLP LCE evident in the photographs in Figure 3c.

A variety of complex free–form LCE objects are printed in **Figure** 4. Each of these free–forms was subjected to uniaxial alignment by subsequent printing and alignment in numerous build layers. In the first example, we printed a 1 mm thick object in the shape of a manta ray. The LCE was aligned laterally across the manta ray. Accordingly, upon heating, the free–form object contracts laterally, resulting in the wings flapping upward (Video S1, Supporting Information). We also printed a 2.5 mm thick LCE snake (Figure 4b). Here, we consecutively printed 25 layers, where alignment is along the length of the snake. Notably, the geometry of the snake and the alignment are decoupled, which is not achievable in the 3D printing of LCEs by DIW. When heated, the snake contracts. Given the orientation of the LCE and the geometry of the shape, this manifests as coiling with the head and tail lifting (Video S2, Supporting Information). As a final illustration, we then printed a 7 mm thick LCE flower-like structure that is mirrored on the top and bottom (Figure 4c). The bottom of the flower was not subjected to alignment while the top of the flower was aligned. This free–form object was prepared in 70 build steps. When heated, the top half of the flower (e.g., aligned) contracts to result in the petals folding in along the alignment direction. Notably, the bottom half of the flower (unaligned) does not deform (Video S3, Supporting Information). Close observation during the heating of the printed free–forms in Figure 4 indicates that the stimuli actuation response seems less as the number of build layers increases. To isolate this, we printed simple rectangular strips with uniaxial alignment from 1 to 70 build layers. For samples less than or equal to 30 layers, strain was measured in tension by DMA. For the 70-layer printed block, the actuation was measured from the change in its length when it was heated. Indeed, as the number of build layers increases, the magnitude of the stimuli-response (e.g., strain) decreases from approximately 25% to 10% (at >30 layers) (Figure S10, Supporting Information). We hypothesize that this decrease is potentially associated with either a change in the magnitude of orientation in subsequent polymerization steps or due to interfacial mechanical losses between build layers.

The studies to this point describe using a single Halbach array arrangement that produces a unidirectional magnetic field (Figure S1a, Supporting Information). Adjusting the orientation of the cube magnets in the Halbach array can generate magnetic fields with complex 2D variance in polarization. This is visualized again with magnetic particles for an additional Halbach array prepared in Figure S1b (Supporting Information). The spatial variance in the magnetic field of this Halbach array is illustrated in **Figure** 5a. Given the association of magnetic field directionality and alignment, we use this array to prepare DLP LCE films with spatial variance in orientation. A single layer DLP LCE was prepared and exhibits an expected saddle-like deformation in Figure 5a. The single-sided (directional) heating and accompanying actuation into a saddle-like configuration are shown in Video S4 (Supporting Information). Spatial variations in director orientation were confirmed with localized WAXS scans (Figure S11, Supporting Information). In the areas where the

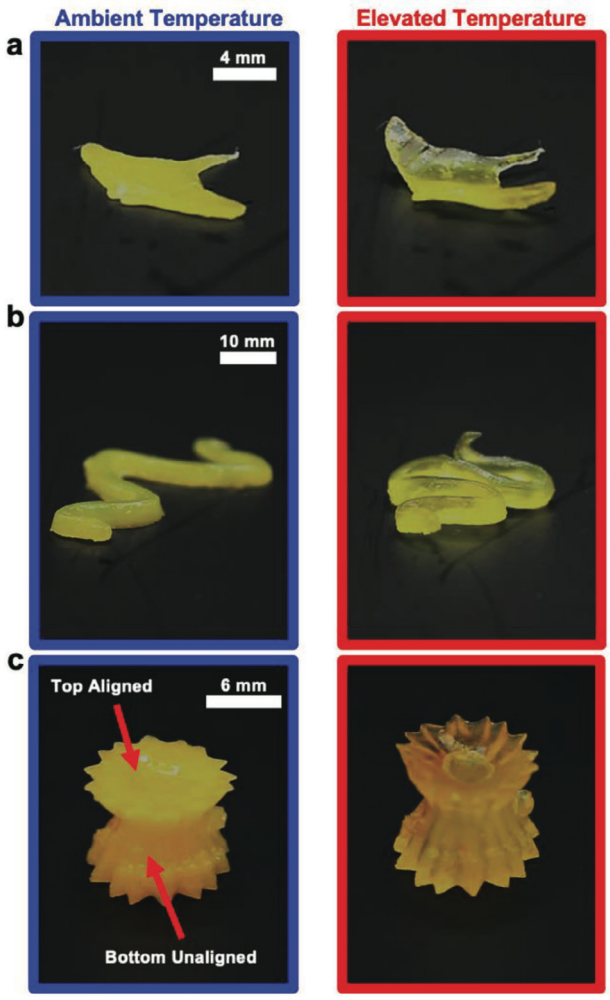

Figure 4. Aligned and DLP printed LCE objects a) A manta ray where the alignment is along the wings. Upon heating, the wings flap. b) A snake where the alignment is parallel to the length of the body. Upon heating, the snake contracts into an attack-like position. c) A 7 mm thick mirrored flower is printed where the bottom half is unaligned and the top is aligned. When heated, only the top of the flower closes.

magnetic strength and directionality are expected to be higher (and where the maximum actuation occurs), WAXS shows clear anisotropy. In the middle of the film, the scan shows an unaligned pattern. Indeed, measuring the magnetic field strength at these locations shows a stronger field at the top and bottom corners and a much weaker field strength in the middle (Figure S11, Supporting Information). Subsequently, we prepared multilayer DLP LCE free–forms with rotation of this alternate Halbach array. Fundamentally, the DLP LCEs have rotation in the nematic director through the material thickness to prepare voxelated free–forms. The printing schematic and stimuli-response of these free–forms are visualized in Figure 5b–d (Supporting Information). Notably, variation in the through-thickness orientation of these materials produces films that can exhibit one or more mechanical instabilities when subject to single-sided (directional) heating. These instabilities are evident in Videos S5–S7 (Supporting Information). These evolving geometries and mechanical instabilities illustrate the versatility of using well-defined and switchable magnetic fields afforded by Halbach arrays.

3. Conclusion

Up to 7 mm thick, aligned LCE free–forms were printed by DLP. The LCE materials chemistry reported here is advantageous in that it is readily amenable to magnetic field alignment and uses main-chain mesogens that significantly enhance the magnitude of the achievable stimuli-response. This report characterizes the fundamentals of magnetic field alignment in both film and free–form elements. From this basis, many layers thick LCE free–forms were prepared by DLP in which alignment was varied between aligned and unaligned, fully aligned, or with through-thickness variance in director orientation. The resulting voxelated LCE free–forms exhibit distinctive stimuli-response including mechanical instabilities. This work advances the opportunity to utilize emerging tools in materials and processing techniques to prepare LCEs in distinctive free–forms that could pilot their functional use in robotics, healthcare, or consumer products.

4. Experimental Section

Materials: The compositions examined here were based on the diacrylate liquid crystalline monomer 1,4-Bis-[4-(6-acryloyloxyhexyloxy)-benzoyloxy]−2-methylbenzene (C6M, Wilshire). C6M was oligomerized by thiol-Michael addition with the dithiol 2,2′-(ethylenedioxy)diethanethiol (EDDT, Aldrich). The thiol-Michael reaction was catalyzed by 1 wt.% of the base catalyst dipropylamine (DPA, Aldrich). Subsequently, the thiol-terminated oligomers were subject to photoinitiated cross-linking by the inclusion of the tetrafunctional vinyl cross-linker glyoxal bis(diallyl acetal) (GDA, Aldrich). Photopolymerization was initiated by 2 wt.% of 2-benzyl-2-dimethylamino-1-(4-morpholinophenyl)-butanone-1 (Irgacure 369, IGM Resins). The radical inhibitor 4-methoxyphenol (MEHQ, Aldrich) was included at 1 wt.% to suppress polymerization before light exposure. The viscosity of the polymerizable compositions was modified by the inclusion of the small molecule liquid crystal 4-Cyano-4′-pentylbiphenyl (5CB, AA Blocks). The UV absorber Sudan I (Aldrich) was mixed at 0.01 wt.% to limit polymerization to the intended build layer in DLP.

Resin Preparation: C6M and 5CB were mixed at a 1:1.5 weight ratio. Other solid components (Irgacure 369 and MEHQ) were weighed and added to the mixture that was melted and mixed. For printed resins, Sudan I was added. Following the addition of solid components, the liquid components (EDDT, GDA, and DPA) were then added. This mixture was vigorously mixed by vortex. The molar ratios between the functional groups were 1.0:1.5:0.5 acrylate:thiol:vinyl. After formulating and mixing, the resin was placed at 100 °C in an oven for three hours to catalyze and expedite the thiol-Michael reaction. The oligomeric composition had distinctive phase behavior and was allowed to cool to room temperature overnight, where it becomes a nematic liquid crystalline resin.

Alignment: For alignment procedures where there is no printing involved, a custom-made Halbach array was printed using fused deposition modeling (FDM) with a platform in the middle of the array to hold the films for alignment and polymerization. For studies with the stronger or weaker magnetic fields, two arrays were made with permanent magnets on opposite sides from each other. Magnets for all studies were purchased from Magnet Shop. For studies where the alignment time was varied, the resin was exposed to the magnetic field for the allotted amount of time before it was exposed to a 385 nm light that locks in the alignment. For studies where the film thickness was controlled, various spacers of 100 to 750 µm were used to control thickness. To remove the 5CB solvent from the cross-linked materials, the films were submerged in DCM for at least 24 h and then allowed to dry before testing.

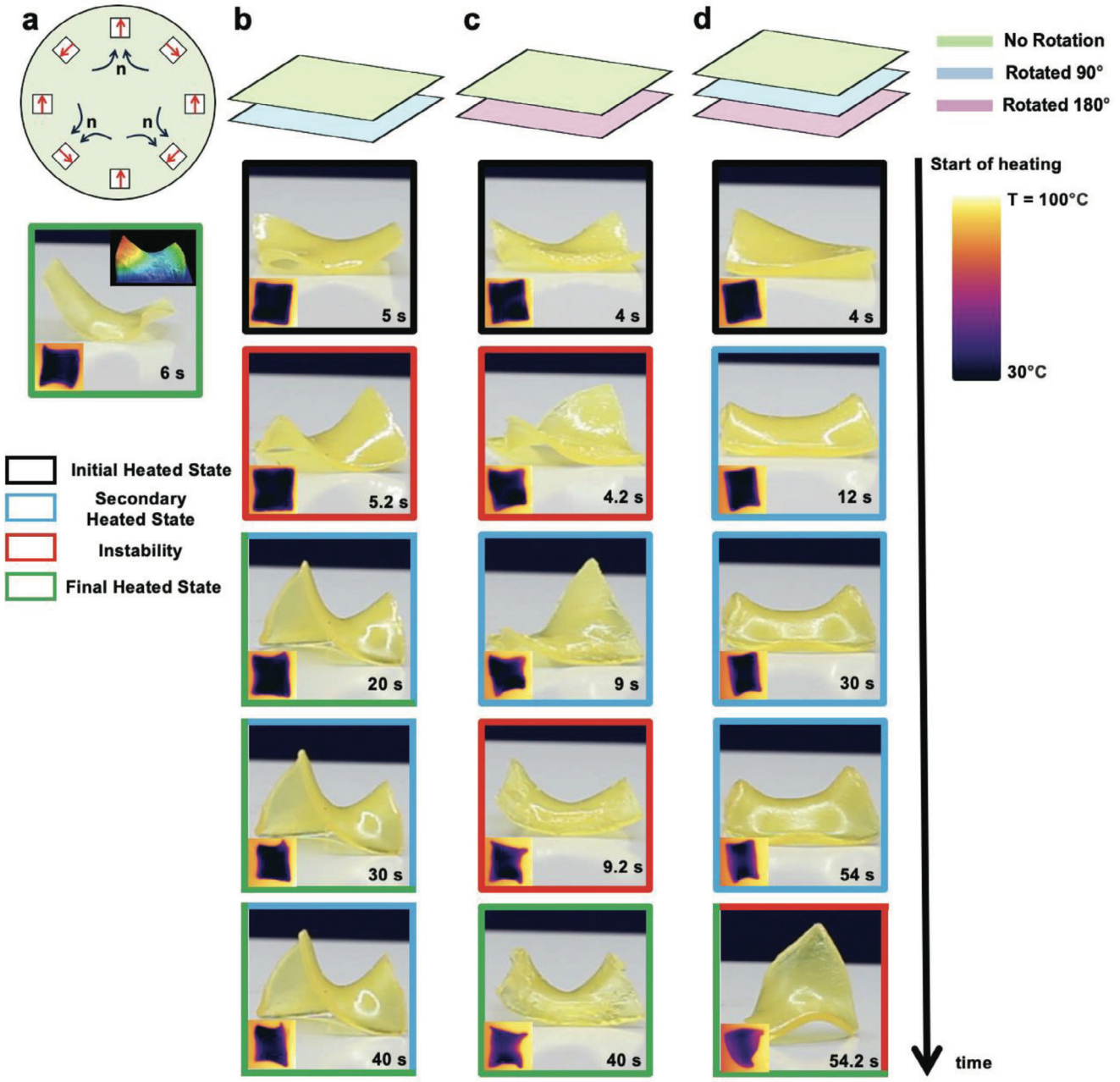

Figure 5. a) An alternate Halbach array was prepared that produces a spatial variance in magnetic field. The spatial variance in orientation of the LCE is evident in the deformation of a single-layer LCE. The deformation away from the hot surface results in a slight thermal gradient (inset). Multilayer 3DP LCE were prepared in which each layer was subsequently oriented in increments of b) 90° (bilayer), c) 180° (bilayer), and d) 90° and 180° (trilayer). The concurrent variation in spatial and hierarchical orientation results in complex mechanical responses including mechanical instabilities. Deformation does contribute to thermal gradients as the elements lift away from the surface (insets).

Characterization: Actuation was characterized in isostress tension experiments via dynamic mechanical analysis (DMA 850 – TA Instruments). Tensile tests and oscillation temperature ramps were also conducted using DMA. Visualization of free-standing actuation of LCE films and free–forms were subject to heating via a heat gun or a hot plate. LCE film morphology was characterized via scanning electron microscopy (SEM) taken on an FEI Helios Nanolab 660 FIB-SEM. LCE samples were freeze-fractured by razor blade after submersion in liquid nitrogen. For SEM imaging, the films were coated with Au/Pd particles. The SEM images shown were taken from the cracked edges. For WAXS experiments, a Xenocs Xeuss 3.0 was used, and scans consisted of a 120 s X-ray exposure with an energy of 8 keV and a sample to detector distance of 43.5 mm. Magnetic field strength was measured using a LATNEX MF-30K AC/DC Gaussmeter and Magnetic Field Indicator.

DLP Printing: A custom-made Halbach array and build stage were FDM printed. In the original file for the Halbach array, a platform was added to the center for film alignment studies. To integrate the array with a DLP printer, this center platform was removed to allow the DLP

build head to pass through the Halbach array unobstructed. The array and build stage were integrated with a commercial DLP printer (Micro DLP, Kudo3D). Control samples without alignment were prepared in the conventional printer system. The oligomerized resin (with 5CB) was poured into the vat. Unless otherwise noted, the resin was allowed to align in the vat for 5 min before printing each build layer. Unless otherwise noted, each printed build layer was 100 µm thick and was exposed to a 385 nm light for 3 s and the dwell time between each layer was set at 5 min. In DLP prints with variation in alignment via adjustment or introduction of alternate Halbach arrays, the resin was allowed to stabilize and align before printing subsequent layers. The lotus flower was designed by Jessica Hogan (jessmakes90, https://www.thingiverse.com/thing:5149723), the manta ray by Finn Clayton (ANudibranch, https://www.thingiverse.com/thing:5314737), the snake by James Sawatsky (IndianaJames, https://www.thingiverse.com/thing:5501261), and the mirrored flower by Luke Johnson (lcjjohnson, https://www.thingiverse.com/thing:4881292).

Supporting Information

Supporting Information is available from the Wiley Online Library or from the author.

Acknowledgements

J.A.H. acknowledges support from the National Science Foundation via a Graduate Research Fellowship. T.J.W. acknowledges support from the National Science Foundation and Air Force Office of Scientific Research. The authors appreciate experimental assistance and consultation with Jonathan Hoang and Joselle McCracken. The authors also acknowledge John Cochrane and Esteban Baca for their help in designing and FDM printing the Halbach array and custom printing stage. Finally, the authors acknowledge Alex Commisso for their helpful tips in DLP printing. This work was performed, in part, at the Center for Integrated Nanotechnologies, an Office of Science User Facility operated for the U.S. Department of Energy (DOE) Office of Science and by the Laboratory Directed Research and Development program at Sandia National Laboratories. Sandia National Laboratories is a multimission laboratory managed and operated by National Technology & Engineering Solutions of Sandia, LLC, a wholly-owned subsidiary of Honeywell International, Inc., for the U.S. DOE's National Nuclear Security Administration under contract DE-NA-0003525. The views expressed in the article do not necessarily represent the views of the U.S. DOE or the United States Government. The authors gratefully acknowledge support from the National Science Foundation through the Harvard MRSEC (DMR-2011754) and the ARO MURI program (W911NF-17-1-03; W911NF-22-1-0219).

Conflict of Interest

The authors declare no conflict of interest.

Data Availability Statement

The data that support the findings of this study are available from the corresponding author upon reasonable request.

Keywords

3D printing, actuation, liquid crystalline elastomers, magnetic alignment, mechanical instabilities

Received: September 19, 2024
Published online: October 29, 2024

[1] Y. Shang, J. Wang, T. Ikeda, L. Jiang, *J. Mater. Chem. C.* **2019**, *7*, 3413.
[2] H. E. Fowler, P. Rothemund, C. Keplinger, T. J. White, *Adv. Mater.* **2021**, *33*, 2103806.
[3] M. O. Saed, W. Elmadih, A. Terentjev, D. Chronopoulos, D. Williamson, E. M. Terentjev, *Nat. Commun.* **2021**, *12*, 6676.
[4] N. A. Traugutt, D. Mistry, C. Luo, K. Yu, Q. Ge, C. M. Yakacki, *Adv. Mater.* **2020**, *32*, 2000797.
[5] C. Luo, C. Chung, N. A. Traugutt, C. M. Yakacki, K. N. Long, K. Yu, *ACS Appl. Mater. Interfaces* **2021**, *13*, 12698.
[6] D. Mistry, N. A. Traugutt, B. Sanborn, R. H. Volpe, L. S. Chatham, R. Zhou, B. Song, K. Yu, K. N. Long, C. M. Yakacki, *Nat. Commun.* **2021**, *12*, 6677.
[7] D. R. Merkel, R. K. Shaha, C. M. Yakacki, C. P. Frick, *Polymer* **2019**, *166*, 148.
[8] S. Y. Jeon, B. Shen, N. A. Traugutt, Z. Zhu, L. Fang, C. M. Yakacki, T. D. Nguyen, S. H. Kang, *Adv. Mater.* **2022**, *34*, 2200272.
[9] M. T. Brannum, A. M. Steele, M. C. Venetos, L. S. T. J. Korley, G. E. Wnek, T. J. White, *Adv. Opt. Mater.* **2019**, *7*, 1801683.
[10] K. R. Schlafmann, T. J. White, *Nat. Commun.* **2021**, *12*, 4916.
[11] K. R. Schlafmann, M. S. Alahmed, K. L. Lewis, T. J. White, *Adv. Func. Mater.* **2023**, *33*, 2305818.
[12] A. T. Phillips, K. R. Schlafmann, H. E. Fowler, T. J. White, *Adv. Opt. Mater.* **2022**, *10*, 2201457.
[13] J. A. Koch, J. A. Herman, T. J. White, *Phys. Rev. Mater.* **2021**, *5*, 62401.
[14] M. Lavrič, N. Derets, D. Črešnar, V. Cresta, V. Domenici, A. Rešetič, G. Skačej, M. Sluban, P. Umek, B. Zalar, Z. Kutnjak, B. Rožič, *Liq. Cryst* **2020**, *48*, 405.
[15] D. Cresnar, N. Derets, M. Trček, G. Skačej, A. Rešetič, M. Lavrič, V. Domenici, B. Zalar, S. Kralj, Z. Kutnjak, B. Rožič, *J. Phys. Energy* **2023**, *5*, 045004.
[16] J. A. Herman, J. D. Hoang, T. J. White, *Small* **2024**, *20*, 2400786.
[17] J. Küpfer, H. Finkelmann, *Makromol. Chem. Rapid Commun.* **1991**, *12*, 717.
[18] M. Warner, P. Bladon, E. Terentjev, *Journal de Physique II* **1994**, *4*, 93.
[19] H. Wermter, H. Finkelmann, *E-Polymers* **2001**, *1*, 013.
[20] S. M. Clarke, A. R. Tajbakhsh, E. M. Terentjev, C. Remillat, G. R. Tomlinson, J. R. House, *J. Appl. Phys.* **2001**, *89*, 6530.
[21] T. H. Ware, M. E. McConney, J. J. Wie, V. P. Tondiglia, T. J. White, *Science* **2015**, *347*, 982.
[22] C. M. Yakacki, M. Saed, D. P. Nair, T. Gong, S. M. Reed, C. N. Bowman, *RSC Adv.* **2015**, *5*, 18997.
[23] C. P. Ambulo, J. J. Burroughs, J. M. Boothby, H. Kim, M. R. Shankar, T. H. Ware, *ACS Appl. Mater. Interfaces* **2017**, *9*, 37332.
[24] A. Kotikian, R. L. Truby, J. W. Boley, T. J. White, J. A. Lewis, *Adv. Mater.* **2018**, *30*, 1706164.
[25] D. J. Roach, X. Kuang, C. Yuan, K. Chen, J. Qi, *Smart Mater. Struct.* **2018**, *27*, 125011.
[26] M. López-Valdeolivas, D. Liu, D. J. Broer, C. Sánchez-Somolinos, *Macromol. Rapid Commun.* **2018**, *39*, 1700710.
[27] X. Peng, S. Wu, X. Sun, L. Yue, S. M. Montgomery, F. Demoly, K. Zhou, R. Zhao, H. J. Qi, *Adv. Mater.* **2022**, *34*, 2204890.
[28] L. McDougall, J. Herman, E. Huntley, S. Leguizamon, A. Cook, T. White, B. Kaehr, D. J. Roach, *ACS Appl. Mater. Interfaces* **2023**, *15*, 58897.
[29] M. Chen, M. Gao, L. Bai, H. Zheng, H. J. Qi, K. Zhou, *Adv. Mater.* **2023**, *35*, 2209566.
[30] S. Li, H. Bai, Z. Liu, X. Zhang, C. Huang, L. W. Wiesner, M. Silberstein, R. F. Shepherd, *Sci. Adv.* **2021**, *7*, 3677.
[31] K. M. Herbert, H. E. Fowler, J. M. McCracken, K. R. Schlafmann, J. A. Koch, T. J. White, *Nat. Rev. Mater.* **2022**, *7*, 23.
[32] Y. Guo, M. Jiang, C. Peng, K. Sun, O. Yaroshchuk, O. Lavrentovich, Q.-H. Wei, *Adv. Mater.* **2016**, *28*, 2353.
[33] K. Ichimura, *Chem. Rev.* **2000**, *100*, 1847.

[34] T. Seki, *Polymer Journal* **2014**, *46*, 751.
[35] A. Münchinger, V. Hahn, D. Beutel, S. Woska, J. Monti, C. Rockstuhl, E. Blasco, M. Wegener, *Adv. Mater. Technol.* **2022**, *7*, 2100944.
[36] S.-J. Ge, T.-P. Zhao, M. Wang, L.-L. Deng, B.-P. Lin, X.-Q. Zhang, Y. Sun, H. Yang, E.-Q. Chen, *Soft Matter* **2017**, *13*, 5463.
[37] D. Rogez, P. Martinoty, *Eur. Phys. J. E.* **2011**, *34*, 69.
[38] C. M. Spillmann, Banahalli, R. R., J. Naciri, *Appl. Phys. Lett.* **2007**, *90*, 021911.
[39] S. Li, M. Aizenberg, M. M. Lerch, J. Aizenberg, *Acc. Mater. Res.* **2023**, *4*, 1008.
[40] M. Tabrizi, T. H. Ware, M. R. Shankar, *ACS Appl. Mater. Interfaces* **2019**, *11*, 28236.
[41] S. Schuhladen, F. Preller, R. Rix, S. Petsch, R. Zentel, H. Zappe, *Adv. Mater.* **2014**, *26*, 7247.
[42] Y. Yao, J. T. Waters, A. V. Shneidman, J. Cui, X. Wang, N. K. Mandsberg, S. Li, A. C. Balazs, J. Aizenberg, *Proc. Natl. Acad. Sci* **2018**, *115*, 12950.
[43] A. Buguin, M.-H. Li, P. Silberzan, B. Ladoux, P. Keller, *J. Am. Chem. Soc.* **2006**, *128*, 1088.
[44] H. Yang, A. Buguin, J.-M. Taulemesse, K. Kaneko, S. Méry, A. Bergeret, P. Keller, *J. Am. Chem. Soc.* **2009**, *131*, 15000.
[45] B. Ni, G. Liu, M. Zhang, P. Keller, M. Tatoulian, M. H. Li, *CCS Chemistry* **2022**, *4*, 847.
[46] C. Ohm, M. Brehmer, R. Zentel, *Adv. Mater.* **2010**, *22*, 3366.
[47] Y. Wang, J. An, H. Kim, S. Jeong, H. Kim, J. Park, S. Ko, J. Son, H. Lee, arXiv **2024**, arXiv:2401.06590.
[48] M. O. Saed, C. P. Ambulo, H. Kim, R. De, V. Raval, K. Searles, D. A. Siddiqui, J. M. O. Cue, M. C. Stefan, M. R. Shankar, T. H. Ware, *Adv. Funct. Mater.* **2019**, *29*, 1806412.
[49] M. O. Saed, E. M. Terentjev, *Sci. Rep.* **2020**, *10*, 6609.
[50] G. E. Bauman, J. M. McCracken, T. J. White, *Angew. Chem., Int. Ed.* **2022**, *61*, 202202577.
[51] D. Dunmur, M. Kaczmarek, T. Sluckin, *Handbook of Liquid Crystals*, Vol. *2*, Wiley, 111 River Street, Hoboken, New Jersey, 07030, USA, **2014**, Chapter 2.
[52] G. E. Bauman, J. D. Hoang, M. F. Toney, T. J. White, *ACS Macro Lett.* **2023**, *12*, 248.
[53] J. A. Herman, J. D. Hoang, J. M. McCracken, T. J. White, *Macromolecules* **2024**, *57*, 664.